Tanzania Journal of Engineering and Technology 2023, **42**(**1**):228-239
OPEN ACCESS articles distributed under Creative Commons Attribution Licence [CC BY-ND]
Websites: https://ajol.org/tjet; https://tjet.udsm.ac.tz

ISSN 1821-536X (**print**); ISSN 2619-8789 (**electronic**)
https://doi.org/10.52339/tjet.v42i1.903

Special Issue – Seventh International Conference on Mechanical and Industrial Engineering (MIE) 2022 Conference, 20 – 21, October 2022, University of Dar es Salaam New Library, Dar es Salaam, TANZANIA

Cellulose-Keratin Supramolecular Composite: Conformation by Combined Fourier Transform Spectroscopy and Partial Least Square Regression Coefficient

Ngesa E. Mushi

Department of Mechanical and Industrial Engineering, College of Engineering and Technology, University of Dar es Salaam, P.O.BOX 35131, Dar es Salaam, Tanzania
Email: mushi.ngesa@udsm.ac.tz

ABSTRACT

Keratin and cellulose are important nano components with excellent mechanical and biological properties. However, the preparation route through dissolution in organic solvents to make manmade materials is challenging because of their intensive bonding interaction characteristics. Structural modification of the natural attributes is difficult to maintain after polymer regeneration. A new technique by a green route was devised to dissolve keratin from wool, hair, and feather with cellulose in situ using 1-Butyl-3-methylimidazolium chloride [BMIm] + Cl- ionic liquid as a solvent. The mixture of keratin and cellulose homogeneously and synergistically resulted in a supramolecular composite film through non-derivatized mechanochemical interactions. The structural properties of α–helix and β-sheets of the regenerated keratin investigated using a Fourier transform spectroscope under transmission mode showed a successful regeneration. Using chemometrics software, the partial least square regression coefficient technique (PLSR) predicted the realistic α–helix and β-sheet content values. Wool showed the highest α–helix, and feathers demonstrated minor content of the secondary structure after regeneration. Regarding the β-sheet form, the feather has regained the most and wool the little content after regeneration. Our data is impressively good compared to the reported results for wool (the highest value was 33 % of the helix for wool) in the literature. The highest values were 52 % for α–helix from wool and 44 % β-sheet for the feather. As expected for all the keratin sources, the α–helix structure decreased, and the β-sheet form increased with the cellulose content. The use of biopolymers and the high temperatures for dissolution is exciting. The preparation route of supramolecular films to achieve multifunctional properties such as strength and biological activities is an inspiration to the green route akin the polymer melt processing techniques.

ARTICLE INFO

First Submitted: Aug. 20, 2022

Revised: Sep. 30, 2022

Presented: Oct. 20-21, 2022

Accepted: Jan. 28, 2023

Published: Feb. 25, 2023

Keywords: *Keratin, cellulose, conformation, regeneration, supramolecular composite, 1-Butyl-3-methylimidazolium chloride*

INTRODUCTION

Animal wastes and by-products are problematic to the environment, and the conversion routes to manmade products for biomedical, cosmeceuticals, and industrial applications are not sustainable. For example, sheep wool, human hair, and chicken feathers, the wastes from fashion, cloths, food processing, poultry, or livestock keeping are rich in biodegradable, renewable, and biocompatible keratin. Keratin shows several biological properties, such as response to antimicrobial activity. Manmade materials based on keratin are essential, especially in administering drug delivery (Tran & Mututuvari, 2015; Vasconcelos & Cavaco-Paulo, 2013), bone replacement, and tissue engineering (Vasconcelos & Cavaco-Paulo 2013). However, brittleness is a problem for regenerated keratin materials, as it is for many proteins, which limits their applications.

Keratin fiber is synthesized in the cytoplasm of mammalian cells, whereby a filamentous protein dies to form a rigid structure. The keratin three-dimensional protein structure is maintained through intensive electrostatic forces, hydrogen bonds, hydrophobic forces, and covalent interactions through disulfide bonds. The peptide bonds provide linkages between individual amino acids (Branden & Tooze, 2012). As a fibrous protein of polypeptide chains arranged in long strands, keratin is an essential biological component in the nails, hair, feathers, quills, wool, scales, tortoises' shells, horns, claws, hooves, and skin of animals (Wang et al. 2016). The keratin from sheep wool, skin, and hair constitutes a soft α-keratin, whereas the β-keratin is hard, like in chicken feathers (Zoccola et al. 2009).

Dissolution and regeneration of biological polymers such as cellulose, hemicelluloses, lignin, chitin, and chitosan allow a bottom-up approach to developing novel materials. Unfortunately, the literature is dominated by common organic solvents such as N-methylmorpholine N-oxide (NMMO) (Krysztof, Olejnik, Kulpinski, Stanislawska, & Khadzhynova, 2018), dimethyl sulfoxide (DMSO) (Dastpak et al., 2020), dimethyl acetamide (DMAc) (Dupont, 2003), chloroform (Purnama & Kim, 2014), acetone, and methanol, which are not environmentally friendly. In addition, the original native structure and properties are also modified, which is somehow not good.

A mechanically robust material is required in, for example, controlled drug delivery, tissue engineering, or pharmaceuticals. Crystalline cellulose dissolved as cellulose I in several aqueous media (Dupont, 2003; Isogai & Atalla, 1998), organic solvents, e.g., DMac/LiCl (Dupont, 2003), and ionic liquids (Kyllönen et al., 2013; Tran & Mututuvari, 2015, 2016) and regenerates into cellulose II with an extended antiparallel chain configuration. The crystalline structure is stiffer (150 GPa) (Sakurada, Nukushina, & Ito, 1962) and stronger (7 GPa) (Wu et al. 2014) than keratin but possesses poor biological properties. On the other hand, keratin is very tough (Wang et al. 2016) and demonstrates good natural properties, mainly controlled drug delivery (Tran & Mututuvari, 2015). Recovering the keratin-intensive bonding interactions responsible for high toughness through a non-derivatized process is difficult compared to cellulose. The combination of keratin and cellulose results in a supramolecular composite and overcomes the mechanical hurdles of the keratin. The Cu-oxam organic-metal complex system ($[Cu(NH_3)_4(OH)_2]$) was reported to dissolve keratin and cellulose (Aluigi, Innocenti, Tonin, Vineis, & Freddi, 2004). However, the work did not study the conformation structure in detail, and the solvent system is not green. Ionic liquids or deep eutectic solvents, such as green solvents, co-dissolve the keratin and cellulose (Arrondo, Muga, Castresana, & Goñi, 1993; Jiang et al., 2018; Kyllönen et al., 2013; Tran & Mututuvari, 2015, 2016; Tran, Prosenc, Franko, & Benzi, 2016). The advantages of ionic liquid are low cost, less environmental impact, and the possibility of upscaling and end-of-life recycling. Supramolecular composites successfully

developed from cellulose and keratin in a single-pot process using butylmethylimidazolium chloride (BMIm+Cl−) ionic liquid showed good mechanical and thermal properties (Tran & Mututuvari, 2015, 2016; Tran et al., 2016). The BMIm+Cl− ionic liquid facilitated cellulose and keratin's chemical stability and compatibility during high-temperature dissolution through a non-derivatized mechanochemical process. Human hair and chicken feather are one of the most challenging proteins to dissolve without disintegrating the secondary structure. No reports have been done to understand the conformation content of the regenerated keratin from hair and chicken feather through dissolution in BMIm+Cl−. The previous work on the structure-property relationship reported well the correlation between the conformation of keratin from chicken feathers, wool, and hair and the mechanical properties of composite films (Tran et al., 2016). Still, it did not give quantitative data on α-helix and β-sheet conformations.

Circular dichroism (DC) and Nuclear Magnetic Resonance (NMR) are suitable for determining the protein's secondary structures, but they are more effective in a liquid phase. A more advanced solid-state NMR technique could be expensive and not practical in low-income countries. The Fourier Transform Infrared (FTIR) method in an attenuated mode employed the deconvolution of the amide bands to predict the α-helix and β-sheet conformation (secondary structures) of a protein structure (Tran & Mututuvari, 2016; Tran et al., 2016). However, the conformation structures obtained strongly depend on the frequency bands' choice; statistically, this data is unreliable. FTIR information combined with a partial least square regression (PLSR) method predicted realistic data for α-helix and β-sheet structure in regenerated wool keratin and the keratin-cellulose composite (Tran & Mututuvari 2016). However, the FTIR mode employed a reflected beam, and using potassium bromide (KBr) pellets in this mode makes it difficult to achieve homogeneously spectral details of the keratin content. As a result, the predicted secondary structure was low (Tran & Mututuvari, 2016) even though the mechanical data and antimicrobial properties favor better recoverable native properties (Tran et al., 2016).

In this work, the secondary structure of keratin from wool, hair, and feather is studied under the transmission mode of an Infrared beam through a thin film of a solid material. Ionic liquid BMIm+Cl− is used as a solvent to co-dissolve cellulose and keratin in a single-pot process. The current objective is to understand better how to predict regenerated keratin's secondary structure conformations more accurately. The previous work investigated the keratin content from sheep wool through attenuated mode. This work has extended a similar technique for wool, hair, and feather keratin by improving the FTIR observation mode, the sample preparation method, and the number of observable samples. A transmitted beam through a solid film is expected to be quantitative and may obtain the secondary structure close to the actual protein conformation based on the FTIR spectral data. The partial least square regression eliminates the possible internal variation of the variables due to the change of the spectral bands or the conformation data. The regeneration of keratin and cellulose inspires the development of polymer melt processes for multifunctional supramolecular composites since high-temperature conditions are involved and through non-derivatized means combined novel properties, preserved biological attributes and functions.

MATERIALS AND METHODS

Materials

The sources of keratin were wool from sheep, human hair, and feathers from a chicken. Wool, hair, and feather were presented as nonwoven microfibrous materials. They were cleaned in acetone/ethanol (1:1) under reflux at 80 °C for 48 hrs to remove organic constituents such as fatty acids, rinsed

vigorously in deionized water, and dried at 80 °C for 48 hrs. The absence of an FTIR band at 1745 cm^{-1} wavenumber from fatty acids confirmed the purity of wool, hair, and feathers. Cellulose from microcrystalline cellulose derived from wood pulp, DP≈ 300 (Battista & Smith, 1962) (Avicel, Sigma Andrich) was used as received. Ionic liquid 1-Butyl-3-methylimidazolium chloride, [BMIm] + Cl-, was prepared in our lab according to the previous procedure (Mututuvari & Tran, 2014; Rosewald, Hou, m Mututuvari, Harkins, & d Tran, 2014; Tran, Duri, & Harkins, 2013).

Methods

Preparation of cellulose-keratin composite films

Thin cellulose-keratin composite films were prepared based on the published protocol (Mututuvari & Tran, 2014; Tran et al., 2013; Tran & Mututuvari, 2016). First, a 0.6 g of solid content (wool, hair, feather, cellulose) was dissolved in 11 g of [BMIm] + Cl- under air atmosphere and mixed in the following manner: 2575, 4060, 5050, 6040, and 7525 cellulose-keratin. Next, wool, hair, and feather were dissolved at 115 - 120 °C temperature for 18 hrs and cellulose at 80 °C for 2 hrs resulting in a viscous solution. The keratin was first dissolved at elevated temperature, and second, continuously added portions of cellulose in the keratin-[BMIm] + Cl- viscous solution under stirring. The dissolution time was fixed for uniformity and comparison between different keratin sources. Then, cellulose and keratin in [BMIm]+ Cl-, viscous solution, was cast on a Mylar sheet (Polyester, McMaster-Carr, Chicago, Illinois) in a homemade Teflon mold, width × length × thickness = 30 × 40 × 0.8 mm (PTFE, McMaster-Carr, Chicago, Illinois) and gelled overnight under atmospheric conditions. The gels were washed several times in ultrapure deionized water until the UV-visible spectral absorbance was co. 0.002 at 209 nm wavelength using UV-VIS spectrophotometer (Perkin Elmer Lambda 35 UV-VIS spectrometer) to remove [BMIm] + Cl altogether- and after that, dried under pressure between filter paper membranes (Whatman Intl Ltd, Maidstone, England) with diameter 90 mm and pore size 6 µm in an oven at 60 °C overnight. Several batches of the composite films were prepared for each composition, such as cellulose wool, cellulose hair, and cellulose feather.

A. Scanning Electron microscope analysis

The topographical surface morphologies of the regenerated cellulose and composite films were examined under vacuum with a JEOL JSM-6510LV/LGS Scanning Electron Microscope (SEM) with standard secondary electrons. Before SEM examination, the film specimens were gold−palladium sputtered by applying a 20 nm coating onto their surfaces using an Emitech K575x Peltier Cooled Sputter Coater (Emitech Products, TX).

Fourier Transform Infra-Red Spectroscopy analysis

For FTIR measurement, thin films were prepared. The thickness of the films ranged from 10 to 35 μm by casting of cellulose-keratin-$[BMIm]^{+}$ Cl^{-} viscous solution. Cellulose-keratin thin film samples were mounted in a sample holder chamber exposed to an infrared beam. The film was scanned 64 times at 2 cm^{-1} resolution under transmission mode, and the spectral curves smoothed 13 times. Absorbance values over a vibration range for amide I and II between 1450 and 1750 cm^{-1} wavenumber were captured to predict of α-helix and β-sheet content.

B. Partial Least Square Regression Analysis

The spectral results were evaluated by PLSR using the chemometrics software (The Unscramble, X10.1, CAMO. Inc., Oslo, Norway) to analyze the keratin conformation statistically, as reported previously (Tran & Mututuvari, 2016). Protein standards of known conformation including BSA (Albumin - Bovin serum), HAS (Albumin – Human serum), HEM (Hemoglobin - Horse), MYO (lysozyme - Chicken egg white), RNASE-A (Ribonuclease A - Bovine pancreas), SOY (Trypsin inhibitor -

Soybean) were used as an internal reference for model development. Before the PLSR analysis, the FTIR spectra were normalized, and the baseline was corrected using origin Pro. The α-helix and β-sheet data were developed from spectral images scanned from at least ten film samples; see a film in Figure 1. The PLSR developed a linear model that correlates the predictor (X) and the response variables (Y) using the least-squares fitting technique as shown in Eq. 1. The predictor variable X contains spectral data from 1450 – 1750 $cm^{-1}$of each of the six protein standards. The response variable Y has information about the secondary structure of the standard proteins.

$$Y = BX \quad (1)$$

where B is the regression coefficient at each frequency, the B values are used to predict the composition of the unknown. The B matrices decomposed to obtain the latent variables that maximize the covariance between X and Y. The secondary structure of the keratin samples were calculated using (2):

$$Y = Bx \quad (2)$$

where x is the spectrum of the unknown protein sample. The settings of the Unscrambler software were such that selected frequency variables closely correlated with the secondary structure.

RESULTS AND DISCUSSION

Preparation of cellulose-keratin composite films

Figure 1 (A, B) presents a photographic image of 6040 cellulose-feather, cellulose-hair, and cellulose-wool composite gels and films. After casting and drying, the images represent a visual impression of the composite samples. The composite gels and films from feathers are translucent, and hair and wool are more transparent. By visual inspection of the background of the images, the feather is very dark, the hair somewhat brown, and the wool film is clearer. The films are mechanically bendable, which is impossible with a pure regenerated keratin film. The composite hydrogels dried under pressure between filter paper membranes arrests molecular mobility during shrinkage and improve aeration to avoid cracking. The dissolution properties are critical for preparing a good film and depend on temperature, time, and molecular weight. The preparation fixed the temperature and time at 115 – 120 °C and 18 hrs for wool, hair, and feather, and 90 – 100 °C and 2 hrs for cellulose dissolution. Wool dissolves faster (~8 hrs) than feathers and hair. The [BMIm] + Cl- solution may be recycled after washing the composite gels.

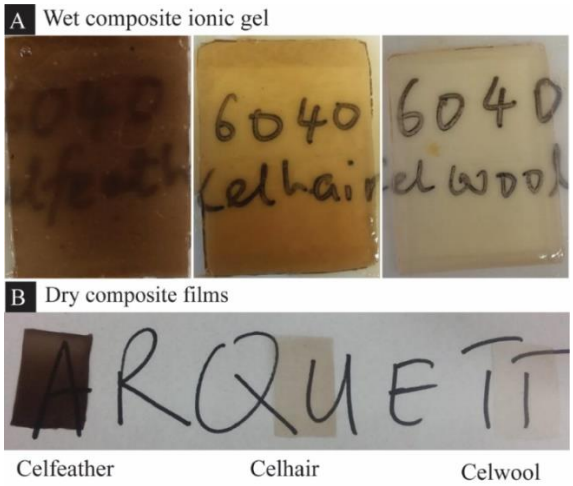

Figure 1: Photographic images of cellulose-keratin gels and films; (A) Wet composite of 60/40 cellulose-feather, cellulose-hair, and cellulose-wool gel on a Mylar sheet, and (B) Cellulose-feather, cellulose-hair, and cellulose-wool films.

Topographical morphology of the composite film

Figure 2 shows the SEM topographical images of the composite films. Figure 2 (A) is a surface of 100% Cel. A smooth surface with homogeneous morphologies is without pores. Cellulose I nanofibrils are regenerated as cellulose II nanofibrils. The nanofibril structures may be observed but are not remarkable at the image resolution. The nanofibrils structure of cellulose II is more apparent in the images of the composite films in Figure 2 (B – J). After mixing with keratin, the regeneration of cellulose and keratin resulted in a rough and porous structure on

the film surface. A similar observation was reported for wool, hair, and chicken feather (Tran et al., 2016). Both keratin and cellulose are hydrophilic biopolymers. The solution of cellulose and keratin showed good chemical compatibility at elevated temperatures in the ionic liquid, hence attributed to the sound dispersion. The surface distribution of keratin and cellulose is homogeneous. The roughness of the surface as keratin content increases relates to the conformation properties of the keratin. The FTIR curves demonstrate that the physical properties are related to non-derivatized mechanochemical interactions associated with the α-helix, β-sheet structure, and cellulose II crystallization. Large-diameter nanofibrils are apparent in celfeather, celhair, and celwool films. Celfeather shows rough surface morphologies with the dominant presence of large-size particles. Celhair and Celwool are dominated by small particle morphologies and swirled nanofibrils, attributed to a smoother surface and transparent films.

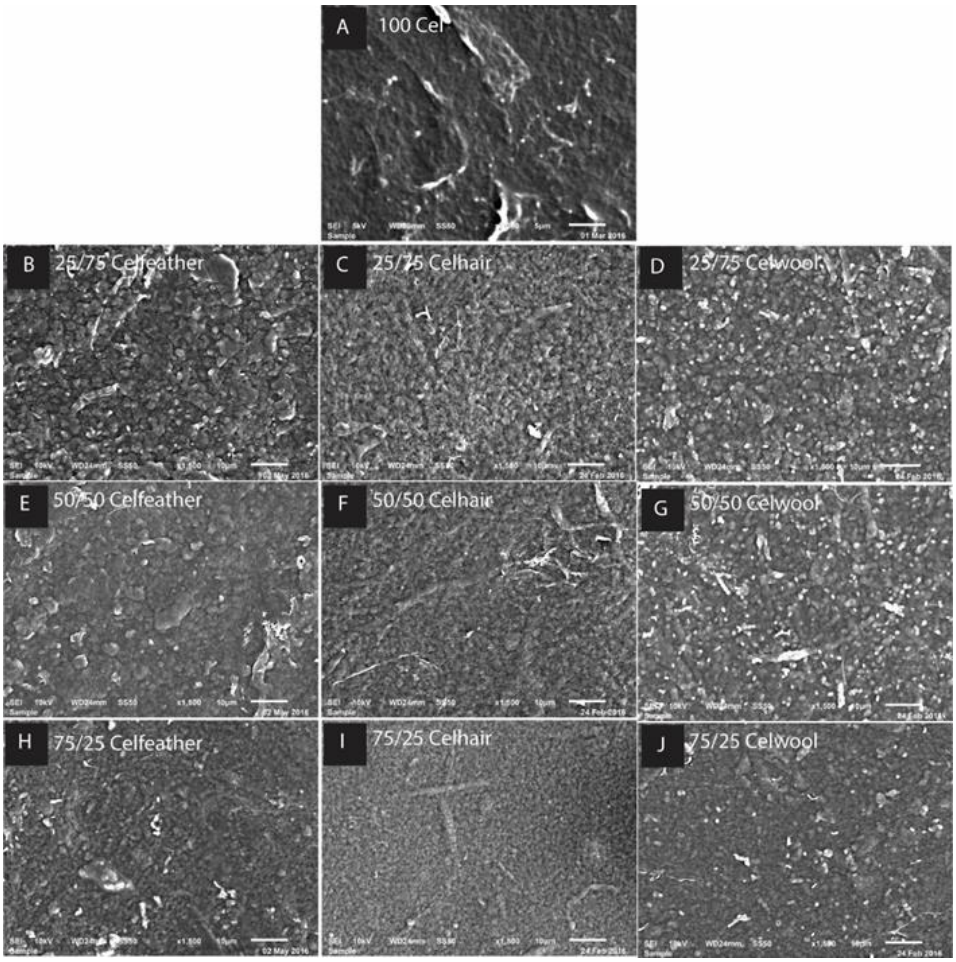

Figure 2: SEM topographical morphologies of the cellulose-keratin supramolecular composite films.

FTIR spectral properties

Figure 3 (A, B, C) represents spectral images of cellulose-keratin composite films at different keratin content. The intensity of absorbance spectra cut off was due to a thicker film for the beam penetration. For the best FTIR spectra under transmission mode, the thickness of the film was around 10 μm. However, better spectral images over the range of 1400 – 1700 cm^{-1} for α-helix and β-sheet prediction by PLSR were possible using a film thickness of up to 35 μm. The

region of interest over 1500 – 1700 cm^{-1} wavenumber attributed to amide I & II is highlighted in a red box in Figure 3 (A, B, C). The spectral bands around 1650 cm^{-1} may be due to C=O stretching from amide I and 1550 cm^{-1} associated with C-N stretching from amide II vibrations (Arrondo et al., 1993). The α-helix and β-sheet spectra appear around 1650−1657 and 1612 − 1640 cm^{-1} wavenumber, respectively (Tran & Mututuvari, 2016).

The absorbance intensity decreases with the decrease in keratin content, which means wool, hair, and feather are somewhat chemically similar in keratin properties. Dispersion and dissolution were most critical during film processing. The correlation between absorbance data and keratin content. The spectral data and the photographic images in Figure 1 confirmed that keratin and cellulose mixed homogeneously, resulting in a flexible composite film. In previous works, wool was employed in cellulose-chitosan-keratin composite films and demonstrated potential for drug delivery and wound healing (Tran & Mututuvari, 2015). It was reported that the peptide bonds (amide I, II) of regenerated wool keratin by ionic liquid was recoverable after regeneration (Tran & Mututuvari, 2016). The current data of keratin spectral characteristics from wool firmly match those of keratin from hair and feather. The regenerated keratin chemical attributes are also expected to preserve the biological properties and mechanical integrity of keratin macromolecular structure (α-helix, β-sheet, and random structures) from feathers and hair. However, the current work did not report the biological properties, such as drug delivery and antimicrobial and mechanical integrity of keratin films or composite films indicates good dissolution and distribution and a successful synergistic non-derivatized mechanochemical interaction through secondary bonds between keratin and cellulose in IL and, after drying, in solid composite films. from hair and feather.

PLSR of cellulose-keratin composite films

The FTIR data of keratin over the 1450 – 1750 cm^{-1} wavenumber predicted the content of α-helix and β-sheet by the PLSR technique, according to Tran and Mututuvari (2016). The PLSR is a multivariate technique to develop models for latent variables (LV) or factors (Lopes, Costa, Alves, & Menezes, 2004). After that, the evaluated model was based on root-mean-square error (RMSE), coefficient of determination (R^2), and the optimal number of LVs. Of noting, the LV is a variable or factor that cannot be observed. However, it can be detected by its effects on observable or measurable variables. In the current work, the calculated factors were to maximize the covariance between the scores of the predictor variables (X), frequency, and the scores of response variables (Y), conformation. The six protein structures of known frequency bands and conformation were used for model validation. The model selected the best fit with the lowest RMSE, highest R^2, and the optimal number of LVs to predict the secondary structure of keratin. Finally, the Jack-knifing method was chosen for cross-model validation (CMV). The CMV model ensured variable selection without overfitting or selecting false variables (Shi, Westerhuis, Rosén, Landberg, & Brunius, 2019). The unobservable internal factors with p-values less than 0.05 for either α-helix or β-sheet are considered significant and were retained in the model.

The model parameter results are published in the previous work (Tran & Mututuvari, 2016). The predicted α -helix and β-sheet content are presented in Figure 4 and Table 1. Figure 4 displays the expected α -helix and β-sheet content against keratin for regenerated wool, hair, and feather in the cellulose-keratin composite films.

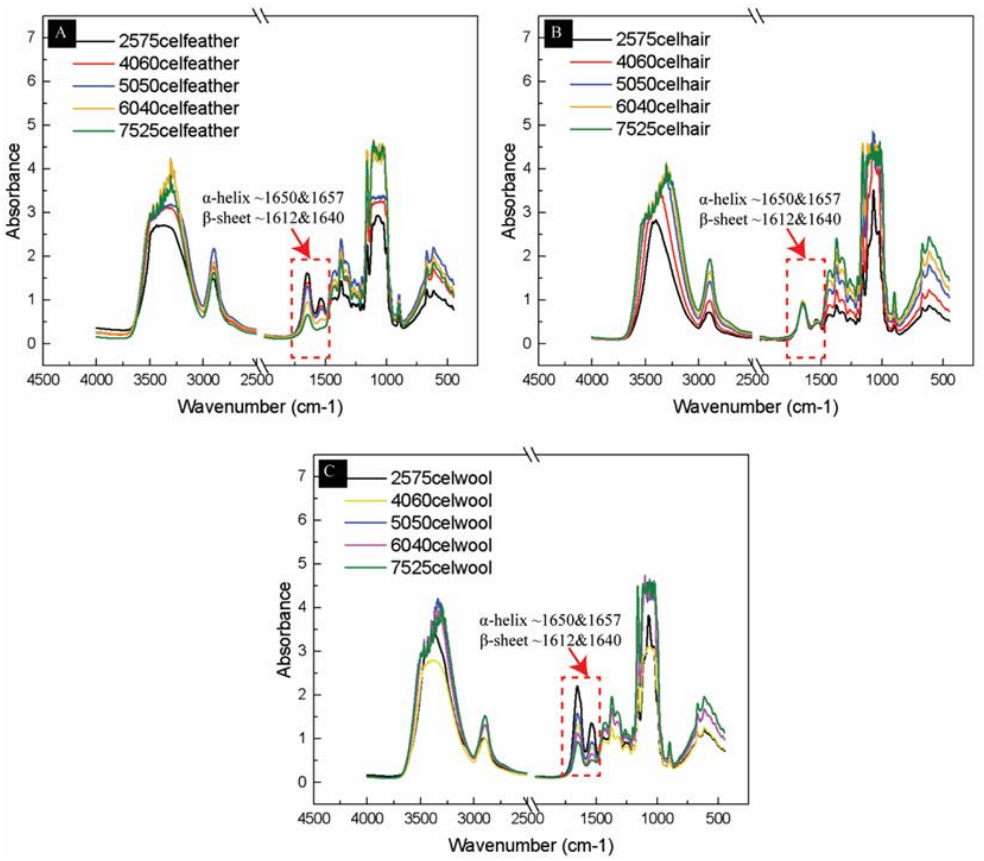

Figure 3: Cellulose-keratin composite films (A) Feather (B) Hair and (C) Wool. The legend provides information of cellulose, wool, hair, and feather composition in the supramolecular film.

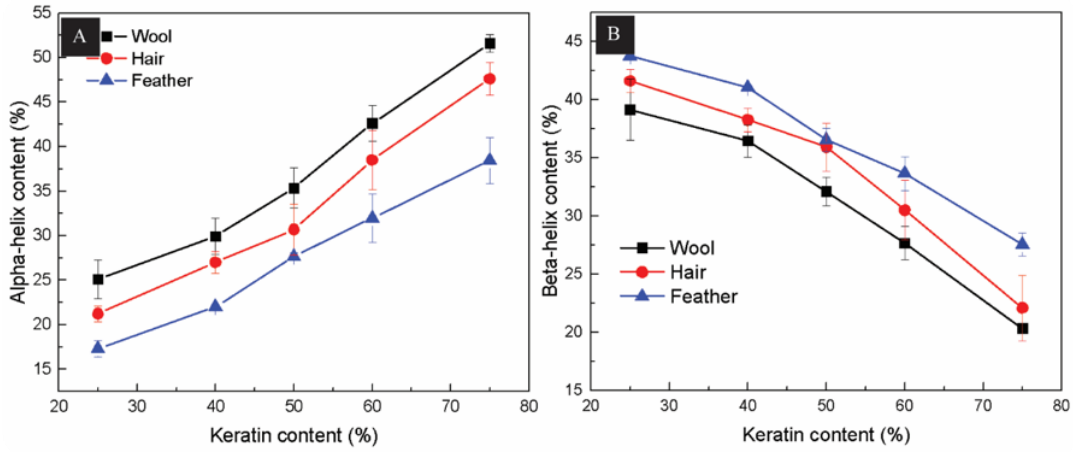

Figure 4: Graphical representation of (A) *α*-helix and (B) *β*-sheet content against keratin content for cellulose-keratin composite films from wool, hair, and feather.

Table 1 summarizes the α-helix and β-sheet content of regenerated keratin in cellulose-keratin composite films and reference materials. Wool shows the highest content of α-helix and the lowest content of β-sheet, followed by hair and feather. A similar observation was reported by Tran et al. (2016) but without quantitative data. The closely related amount of α-helix and β-sheet content in wool, hair, and feather is attractive. For example, α-helix content for the 2575 cellulose-keratin samples was 52 %, 48 %, and 38 % for wool, hair, and feather, respectively. The reasons for this are unclear

but may be attributed to the cysteine di-sulfide content that differentiates between keratin-based biological materials. On average, about 70 % of the keratin total conformations were successfully regenerated in the composite films, which is a good achievement so far. The remaining 30 % are the random conformations. By comparing to the SEM topographical morphologies in Figure 2, the nature of the particle aggregates of the celfeather, celhair, and celwool draw to the keratin conformation data. The α-helix rich content in wool and hair, presented as a rougher morphology, seems better to promote extended nanofibril cellulose in the composite matrix. On the other hand, the β-sheet appeared to influence the formation of fibril aggregates in the presence of regenerated cellulose. The particle morphologies in the composite films are an interesting observation. The variation of keratin conformation will project different biological properties, and this is an avenue for, for example, drug release control and mechanical properties tailoring. The current data shows higher content of α-helix for wool, e.g., at 2575 cellulose-keratin content, compared to the previous work (Tran & Mututuvari, 2016). See the reference sample 2575*** in Table 1. The overall total conformation recoverable increased from around 50 % to 79 % in the current work. It is not easy to form a pure keratin film because of embrittlement. The low molecular weight or poor plasticization effect of keratin in the dry state is a problem. KBr pellets under attenuated mode in the FTIR analyzed the pure wool sample (Tran & Mututuvari, 2016; Tran et al., 2016). The predicted α-helix content of the composite films is higher than that of pure wool (32 %).

The FTIR spectral analysis under transmission mode improved the data quality as expected since the beam passes through a more homogeneous sample. The PLSR is proved to be especially useful when the predictor variables (wavenumber or frequency) are highly collinear or affect each other or when the number of observable and non-observable predictors is highly improbable and when the ordinary least-squares regression technique produces coefficients with high standard errors.

In a composite film Figure 3, a strong correlation is exhibited between the keratin content and secondary conformation responses (α-helix and β-sheet). α-Helix content increases with the increase in keratin content, whereas β-sheet content decreases with the rise in keratin content. However, the correlation is not linear and does not follow the same trend for wool, hair, and feather. Therefore, the unknown conformations may be grouped under random conformation.

Table 1: Table of α-helix and β-sheet content of cellulose-keratin composite by PLSR and FTIR transmission over the spectra range 1450 – 1750 cm^{-1} through solid films.

Compositions of cellulose- keratin	Wool		Hair		Feather	
	α-helix %	β-sheet %	α-helix %	β-sheet %	α-helix %	β-sheet %
2575	52 (1)	20 (1)	48 (2)	22 (3)	38 (3)	28 (1)
4060	43 (2)	28 (1)	39 (4)	31 (3)	32 (3)	34 (2)
5050	35 (2)	32 (1)	31 (3)	36 (2)	28 (1)	37 (1)
6040	30 (2)	36 (1)	27 (1)	38 (1)	22 (1)	41 (1)
7525	25 (2)	39 (3)	21 (1)	42 (1)	17 (1)	44 (1)
100Wool*	33 (2)	18 (0.4)	-	-	-	-
100Keratin**	31 (8)	21 (3)	-	-	-	-
2575***	32 (9)	25 (4)	-	-	-	-

Note: Samples with *, **, *** are from Tran and Mututuvari (2016). Sample *** is a regenerated cellulose-keratin composite film.

The inconsistency of the conformation data may arise from protein and cellulose dispersion during mixing and casting or due to poor dissolution of the protein. For example, hair and feather were more complicated and required extended time to dissolve than wool. Moreover, the wool, hair, and feather conformation are also not the same. Thus, it is unclear to the author if the current data of α-helix and β-sheet content for wool, hair, and feather is within the range of most biological materials. Previously, the secondary structure of native wool was around 33 % α-helix and 18 % β-sheets through attenuated mode and KBr pellets FTIR analyzed data (Tran & Mututuvari, 2016). In a deep eutectic solvent of choline chloride-urea, the amount of α-helix of regenerated wool keratin was around 48.6 % (Jiang et al., 2018). Much higher values are reported based on the current predictions.

CONCLUSIONS

The present work studied the conformation content of regenerated keratin from wool, hair, and feather after using [BMIm] + Cl- ionic liquid as a solvent and drying to form solid cellulose-keratin composite films. The most critical parameters in film preparation included the keratin and cellulose dissolution temperature and time. Thin cellulose-keratin composite films showed somewhat mechanical flexibility and transparency. Cellulose and keratin from wool, hair, and feather mixed homogeneously and synergistically through non-derivatized mechanochemical interactions. The FTIR data were related to the previous data and showed that α-helix and β-sheet content is higher in the current work, 52 % compared to 31 % α-helix content for 2575 cellulose-wool. FTIR spectra in transmission mode were successfully employed with the PLSR to analyze and predict α-helix and β-sheet secondary structure content. A composite film of around 25 μm thick gives better FTIR absorbance spectral data. The PLSR and observation through a transmission mode are crucial to eliminating errors from unobservable parameters. The conformation data suggests that the significant native properties of keratin are recoverable after regeneration compared to the previous works. Our data suggest about 70 % on average of α-helix and β-sheet content are recoverable from the keratin sources. These data are the most realistic for α-helix and β-sheet content in the regenerated cellulose-keratin composite films. Concerning α-helix content, wool has the most and feathers the least, and regarding β-sheet content, the feather has the most and wool the least. The current work is an inspiration to prepare supramolecular hybrid films with multifunctional properties such as strength and biological activities and also invokes a vital challenge on green routes and polymer melt processing techniques in the aspect of natural or biological polymeric materials.

ACKNOWLEDGMENT

The author thanks Marquette University at Milwaukee USA for funding this project and Prof. Chieu Tran for the postdoctoral opportunity.

REFERENCES

Aluigi, A., Innocenti, R., Tonin, C., Vineis, C., & Freddi, G. (2004). Studies on keratin/cellulose films from cuprammonium solution. *Autex Research Journal*, **4**(4): 174--180.

Arrondo, J. L. R., Muga, A., Castresana, J., & Goñi, F. M. (1993). Quantitative studies of the structure of proteins in solution by Fourier-transform infrared spectroscopy. *Progress in biophysics and molecular biology*, **59**(1): 23-56. doi:https://doi.org/10.1016/0079-6107(93)90006-6

Battista, O., & Smith, P. (1962). Microcrystalline cellulose. *Industrial & Engineering Chemistry*, **54**(9): 20-29. doi:https://doi.org/10.1021/ie50633a003

Branden, C. I., & Tooze, J. (2012). *Introduction to protein structure*: Garland Science.

Dastpak, A., Lourençon, T. V., Balakshin, M., Hashmi, S. F., Lundström, M., & Wilson,

B. P. (2020). Solubility study of lignin in industrial organic solvents and investigation of electrochemical properties of spray-coated solutions. *Industrial crops and products*, **148**: 112310. doi:https://doi.org/10.1016/j.indcrop.2020.112310

Dupont, A.-L. (2003). Cellulose in lithium chloride/N, N-dimethylacetamide, optimisation of a dissolution method using paper substrates and stability of the solutions. *Polymer*, **44**(15): 4117-4126. doi:https://doi.org/10.1016/S0032-3861(03)00398-7

Isogai, A., & Atalla, R. (1998). Dissolution of cellulose in aqueous NaOH solutions. *Cellulose*, **5**(4): 309-319. doi:https://doi.org/10.1023/A:1009272632367

Jiang, Z., Yuan, J., Wang, P., Fan, X., Xu, J., Wang, Q., & Zhang, L. (2018). Dissolution and regeneration of wool keratin in the deep eutectic solvent of choline chloride-urea. *International journal of biological macromolecules*, **119**: 423-430. doi:https://doi.org/10.1016/j.ijbiomac.2018.07.161

Krysztof, M., Olejnik, K., Kulpinski, P., Stanislawska, A., & Khadzhynova, S. (2018). Regenerated cellulose from N-methylmorpholine N-oxide solutions as a coating agent for paper materials. *Cellulose*, **25**(6): 3595-3607. doi:https://doi.org/10.1007/s10570-018-1799-y

Kyllönen, L., Parviainen, A., Deb, S., Lawoko, M., Gorlov, M., Kilpeläinen, I., & King, A. W. (2013). On the solubility of wood in non-derivatising ionic liquids. *Green chemistry*, **15**(9): 2374-2378. doi:10.1039/C3GC41273C

Lopes, J. A., Costa, P. F., Alves, T. P., & Menezes, J. C. (2004). Chemometrics in bioprocess engineering: process analytical technology (PAT) applications. *Chemometrics and Intelligent Laboratory Systems*, **74**(2): 269-275. doi:https://doi.org/10.1016/j.chemolab.2004.07.006

Mututuvari, T. M., & Tran, C. D. (2014). Synergistic adsorption of heavy metal ions and organic pollutants by supramolecular polysaccharide composite materials from cellulose, chitosan and crown ether. *Journal of hazardous materials*, **264**: 449-459. doi:https://doi.org/10.1016/j.jhazmat.2013.11.007

Purnama, P., & Kim, S. H. (2014). Biodegradable blends of stereocomplex polylactide and lignin by supercritical carbon dioxide-solvent system. *Macromolecular Research*, **22**(1): 74-78. doi:https://doi.org/10.1007/s13233-014-2004-2

Rosewald, M., Hou, F. Y. S., m Mututuvari, T., Harkins, A., & d Tran, C. (2014). Cellulose-chitosan-keratin composite materials: synthesis, immunological and antibacterial properties. *ECS transactions*, **64**(4): 499. doi:10.1149/06404.0499ecst

Sakurada, I., Nukushina, Y., & Ito, T. (1962). Experimental determination of the elastic modulus of crystalline regions in oriented polymers. *Journal of Polymer Science*, **57**(165): 651-660. doi:https://doi.org/10.1002/pol.1962.1205716551

Shi, L., Westerhuis, J. A., Rosén, J., Landberg, R., & Brunius, C. (2019). Variable selection and validation in multivariate modelling. *Bioinformatics*, **35**(6): 972-980. doi:https://doi.org/10.1093/bioinformatics/bty710

Tran, C. D., Duri, S., & Harkins, A. L. (2013). Recyclable synthesis, characterization, and antimicrobial activity of chitosan-based polysaccharide composite materials. *Journal of biomedical materials research Part A*, **101**(8): 2248-2257. doi: https://doi.org/10.1002/jbm.a.34520

Tran, C. D., & Mututuvari, T. M. (2015). Cellulose, chitosan, and keratin composite materials. Controlled drug release. *Langmuir*, **31**(4): 1516-1526. doi:https://doi.org/10.1021/la5034367

Tran, C. D., & Mututuvari, T. M. (2016). Cellulose, chitosan and keratin composite materials: Facile and recyclable synthesis, conformation and properties. *ACS sustainable chemistry & engineering*, **4**(3): 1850-1861. doi:https://doi.org/10.1021/acssuschemeng.6b00084

Tran, C. D., Prosenc, F., Franko, M., & Benzi, G. (2016). Synthesis, structure and antimicrobial property of green composites from cellulose, wool, hair and chicken feather. *Carbohydrate Polymers*, **151**: 1269-1276. doi:https://doi.org/10.1016/j.carbpol.2016.06.021

Vasconcelos, A., & Cavaco-Paulo, A. (2013). The use of keratin in biomedical applications. *Current drug targets*, **14**(5): 612-619. doi:10.2174/1389450111314050010.